NON-LINEAR DEFLECTION ANALYSIS OF A SPACE SUIT WAIST BEARING

J. C. Lambert, Structural Analyst, Applied Mechanics
W. M. Merritt, Head of Applied Mechanics, Space and Sea Systems

United Technologies Corporation
Hamilton Standard Division
1 Hamilton Road
Windsor Locks, CT 06096

I. Abstract:

A deflection analysis of a space suit waist bearing has been conducted using MSC/NASTRAN. The space suit waist bearing is a ball bearing, about 15.5 inches in diameter, subject to axial point loading due to suit pressure and man loads. Using CGAP elements and SOL66, the non-linear stiffening effects of this bearing were considered. Evaluation of these non-linear stiffening effects is necessary for proper calculation of radial and axial deflections which are important in the design of space suit seals.

This paper outlines the complexities of the space suit waist bearing and the analysis technique used to investigate its behavior. It also highlights the results of the analysis and demonstrates, under various load conditions, how changes in ball contact angle affect overall bearing stiffness. This analysis technique enables designers to understand the behavioral characteristics of deflection sensitive bearings without

costly prototype development.

II. Introduction:

The space suit is a system of components that allows an astronaut to maneuver in the vacuum environment of outer space. This suit is composed of many components and assemblies that provide the astronaut with a pressurized environment and allow the astronaut to move freely while in the suit. One of the major assemblies that provide such mobility is the lower torso assembly (LTA). An important part of this assembly is a large diameter waist bearing that allows free rotation of the astronaut's hips (Figure 1). The waist and brief (Figure 1) are tied together through the use of this bearing.

The space suit waist bearing is a ball bearing consisting of approximately 15.5 inch diameter races. Above and below both races are garment clamping rings that bolt into the races (Figure 2). These rings secure the suit fabric to the races and provide for a pressure tight seal. Between the two races is a pressure seal which prevents leakage of oxygen gas from the suit.

Due to suit pressure, loads are created that try to separate the waist from the brief. As a result the outer race, which is fastened to the waist, is subject to two thrust point loads located 180 degrees apart. The inner race, which is fastened to the brief, is subject to four point loads located 90 degrees apart (Figure 3). This peculiar loading and bearing geometry result in a system that behaves in a non-linear manner and is difficult to understand without the use of computer analysis. A thorough understanding of the bearing's behavior under load is critical due to the stringent operating requirements of this compo-

LOWER TORSO ASSEMBLY

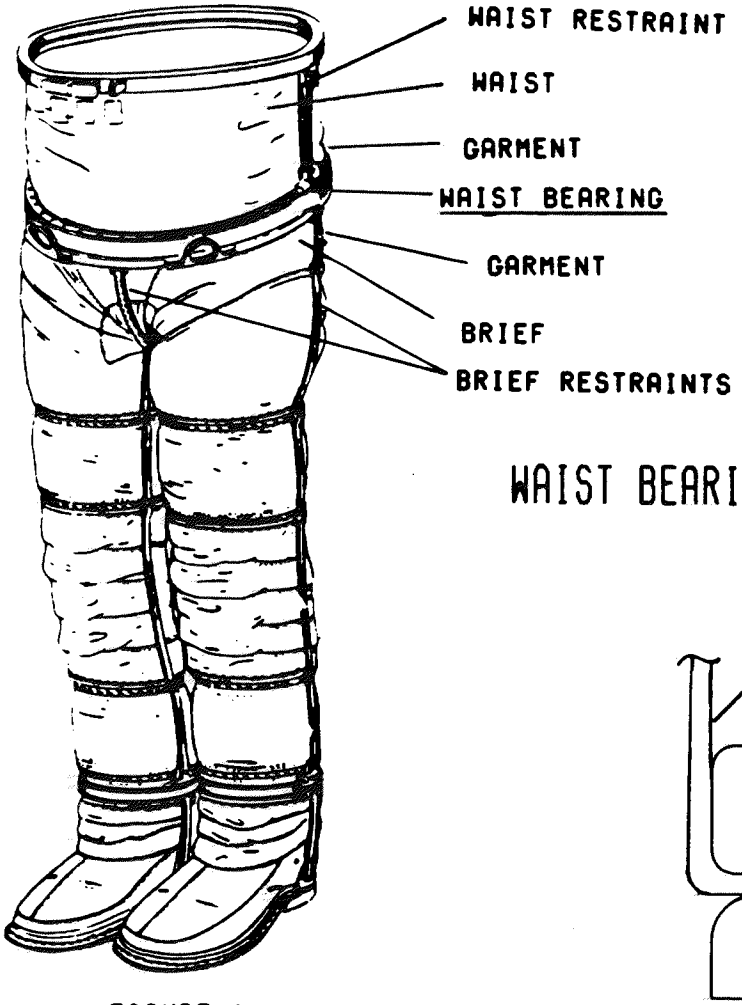

FIGURE 1.

WAIST BEARING ASSEMBLY CROSS SECTION

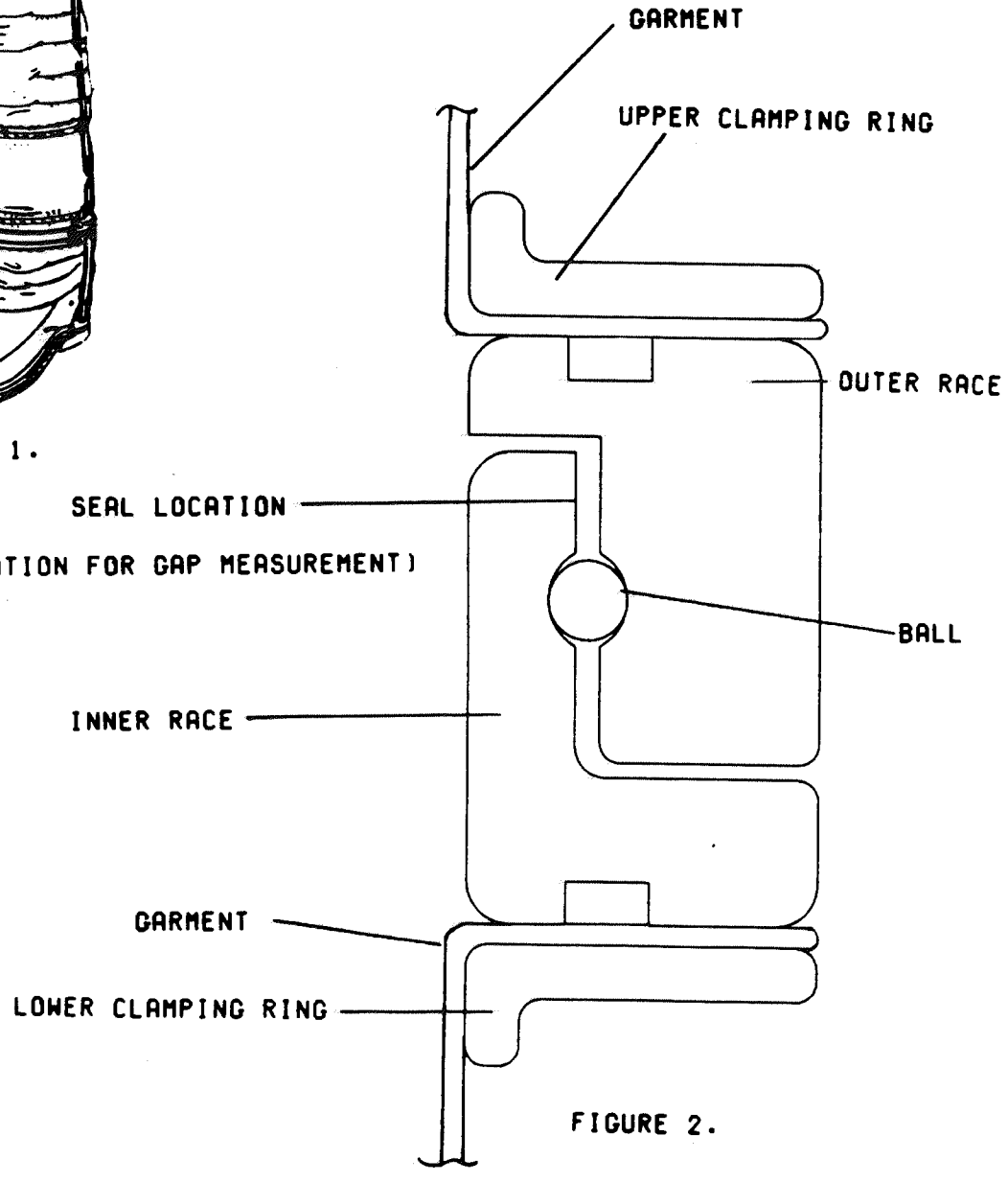

FIGURE 2.

WAIST BEARING

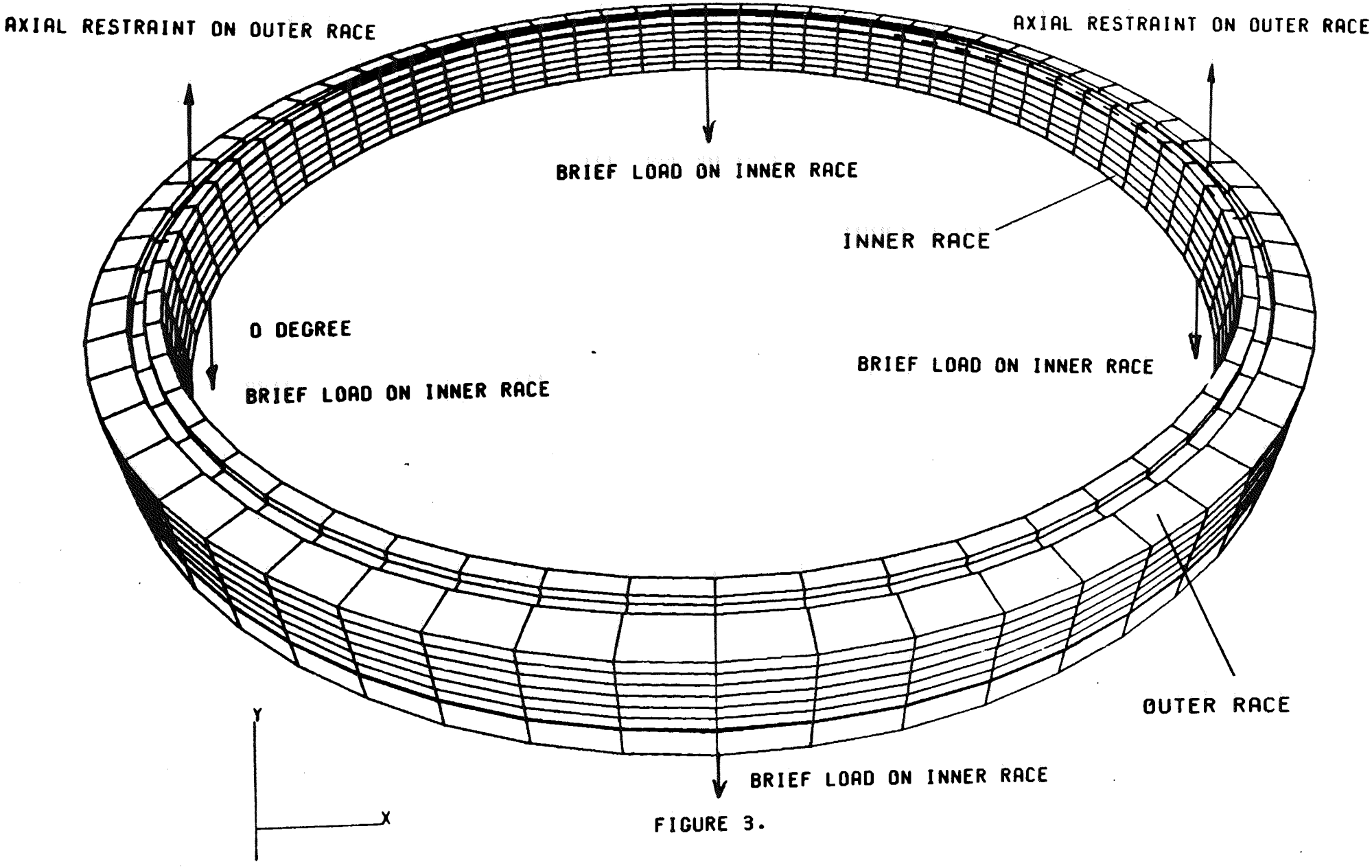

FIGURE 3.

nent. This understanding, until recently, was limited to information attained from hand calculations and tests.

The waist bearing has a number of complexities that must be understood for proper design. Ball contact angle is important because of the low torque requirements of the bearing. The change in ball contact angle is also important because it is directly related to changes in radial gap between the two races (Figure 2). This gap is of interest for optimum seal squeeze design, another factor in bearing operating torque (Figure 2). Ball loading is necessary information in order to calculate ball/race contact stresses. Ball loading distribution is also useful in identifying "floating" balls, balls that do not carry any load. Floating balls are of interest in the study of ball blocking [1]. These are some of the problem complexities that the analysis had to account for.

Information from this analysis will be used to make certain modifications to the existing design. Seal squeeze, which is the amount the seal is compressed between the races, will be optimized. The ball loading distribution will be altered in order to reduce localized ball load peaks and axial and radial deflection will be controlled to maintain a fairly constant contact angle as the bearing rotates.

III. Analysis Procedure.

An initial solid model of the bearing assembly was created (Figure 4). This model had CBAR elements to represent balls and had a fixed contact angle of 45 degrees (Figure 5). The appropriate loads were applied and the model was run. This model had limitations in that the outer race, due to radial ball loadings, deflected excessively relative to the inner race in the radial direction (Figure 6). The deflection would

BEARING ASSEMBLY

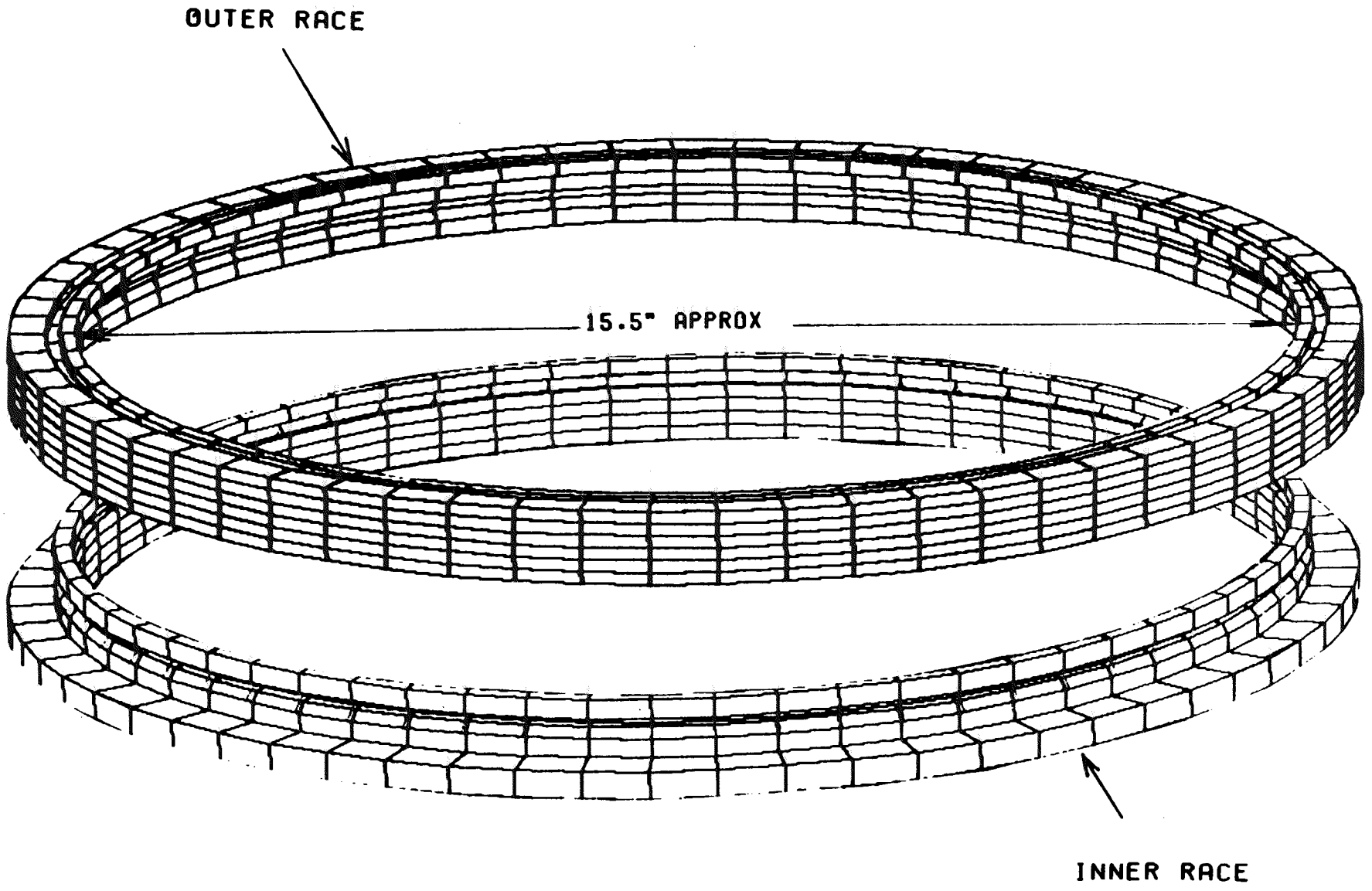

FIGURE 4.

BEARING MODEL CROSS SECTION

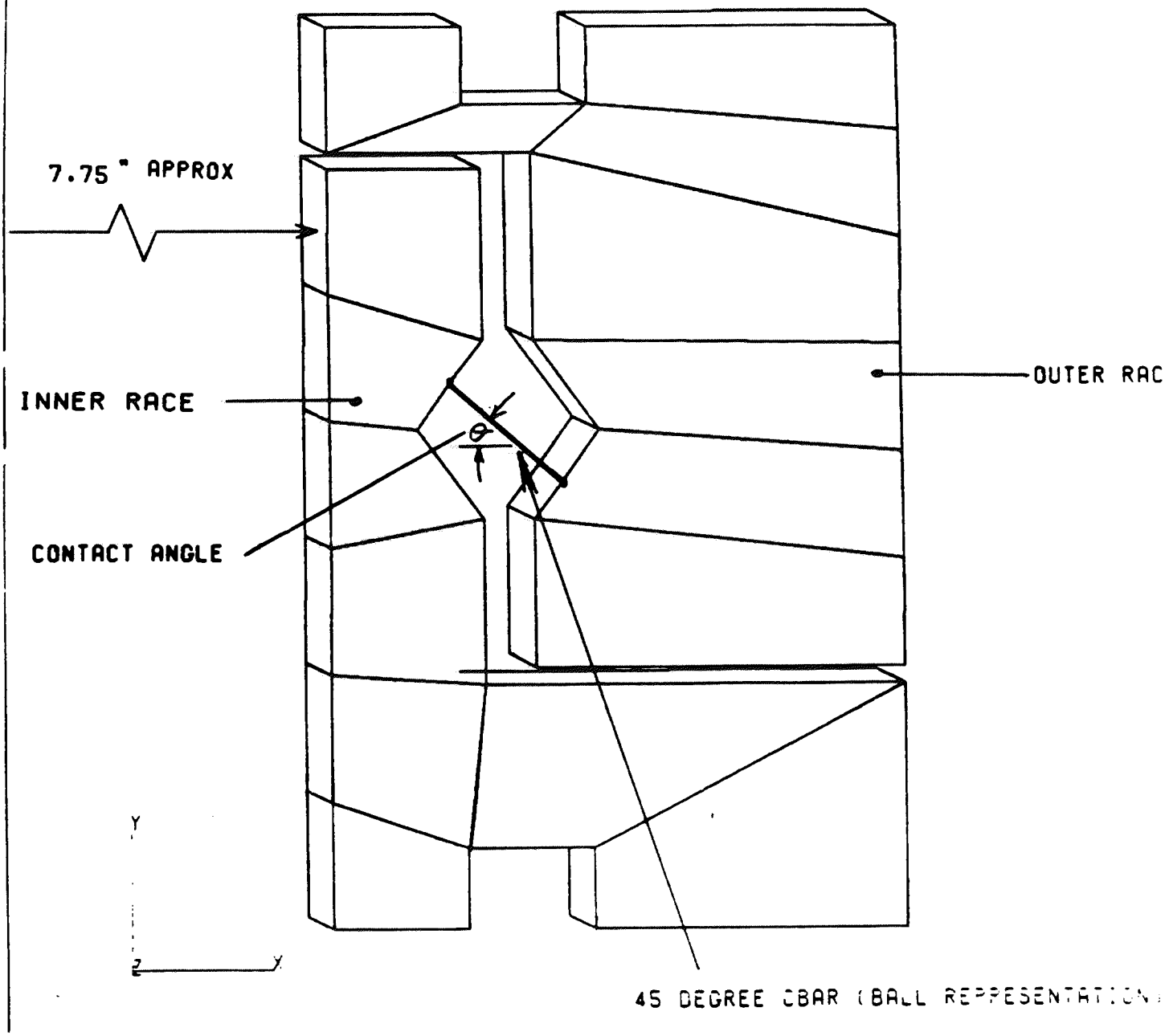

FIGURE 5.

EXAGERATED DEFLECTIONS

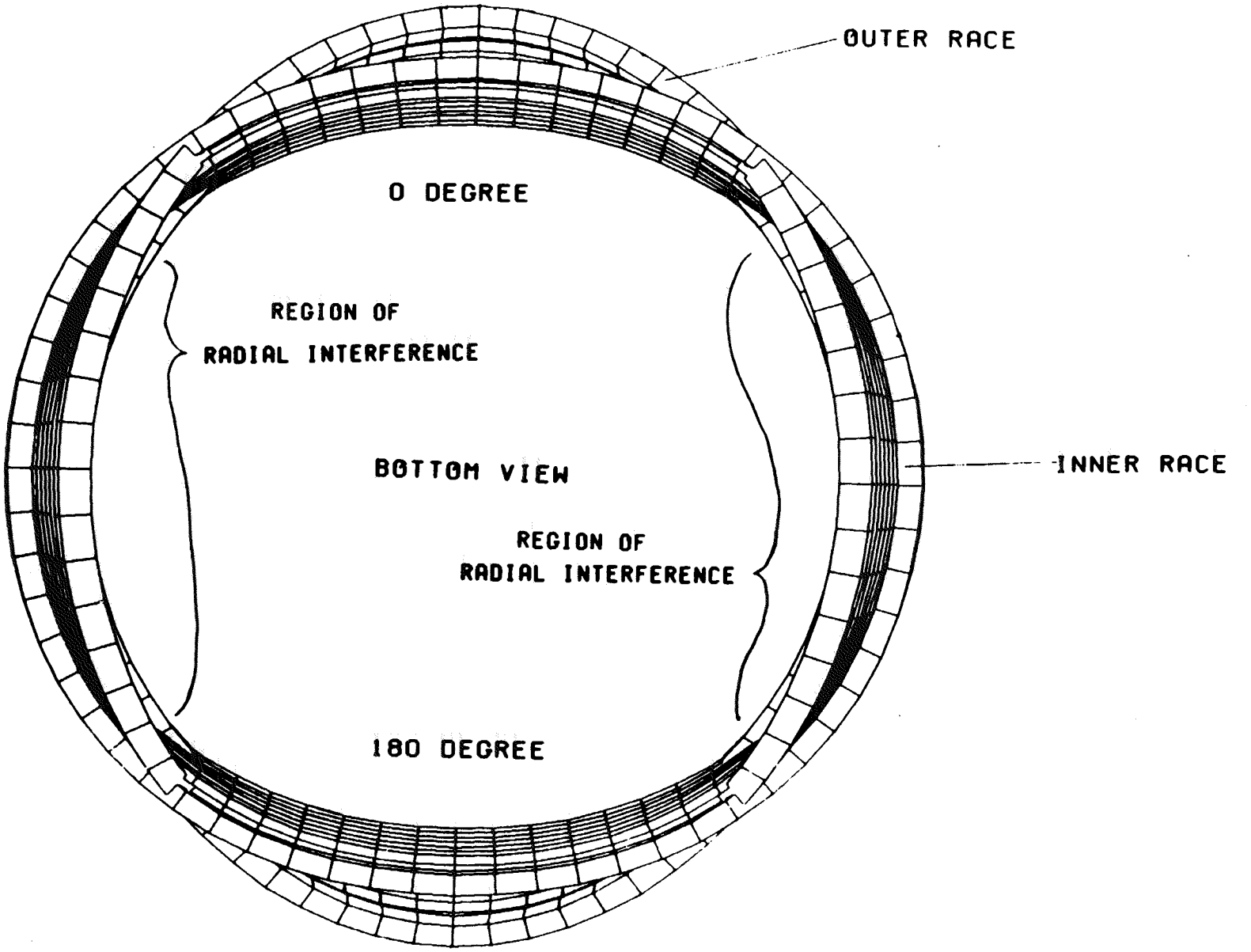

FIGURE 6.

normally be restricted by the presence of balls (Figure 7). To account for this interference CBAR elements were placed across the races in a zero degree contact orientation. This was done over the entire 360 degrees of the bearing. The model was run and any of the radial CBARS that went into tension were removed. This process was repeated until the proper range of radial interference was determined. This method, although effective, was time consuming, costly and had to be repeated every time the model was changed. In addition it represented a zero clearance condition between the balls and the races. As a result, the decision was made to use CGAP elements to represent the radial interference of the races.

The use of CGAP elements provided capability to consider the radial gap closing without manually iterating to find the range. These elements also allowed for modeling of the actual ball/race clearances, rather than a zero clearance bearing. This technique proved to be quite successful in that the non-linear solution ran with relative ease and the results correlated very well with those from the previous solution techniques. The flaw in this method was that with the 45 degree CBARS, the closing of a gap element created a rigid truss between the races. This caused tensile loading of some of the CBARS, a condition not possible in the actual bearing. From radial race deflections, ball contact angle was back calculated. It can been seen from figure 7 that a line drawn through the race centers determines the contact angle. This angle can easily be calculated using the total distance, the triangle hypotenuse, and the radial distance between these centers. The total distance, which is equal to 2 times the difference between the ball radius and the race radius, is predetermined by the bearing geometry and remains constant. The radial distance is a function of relative race location and is

BALL/RACE GEOMETRY

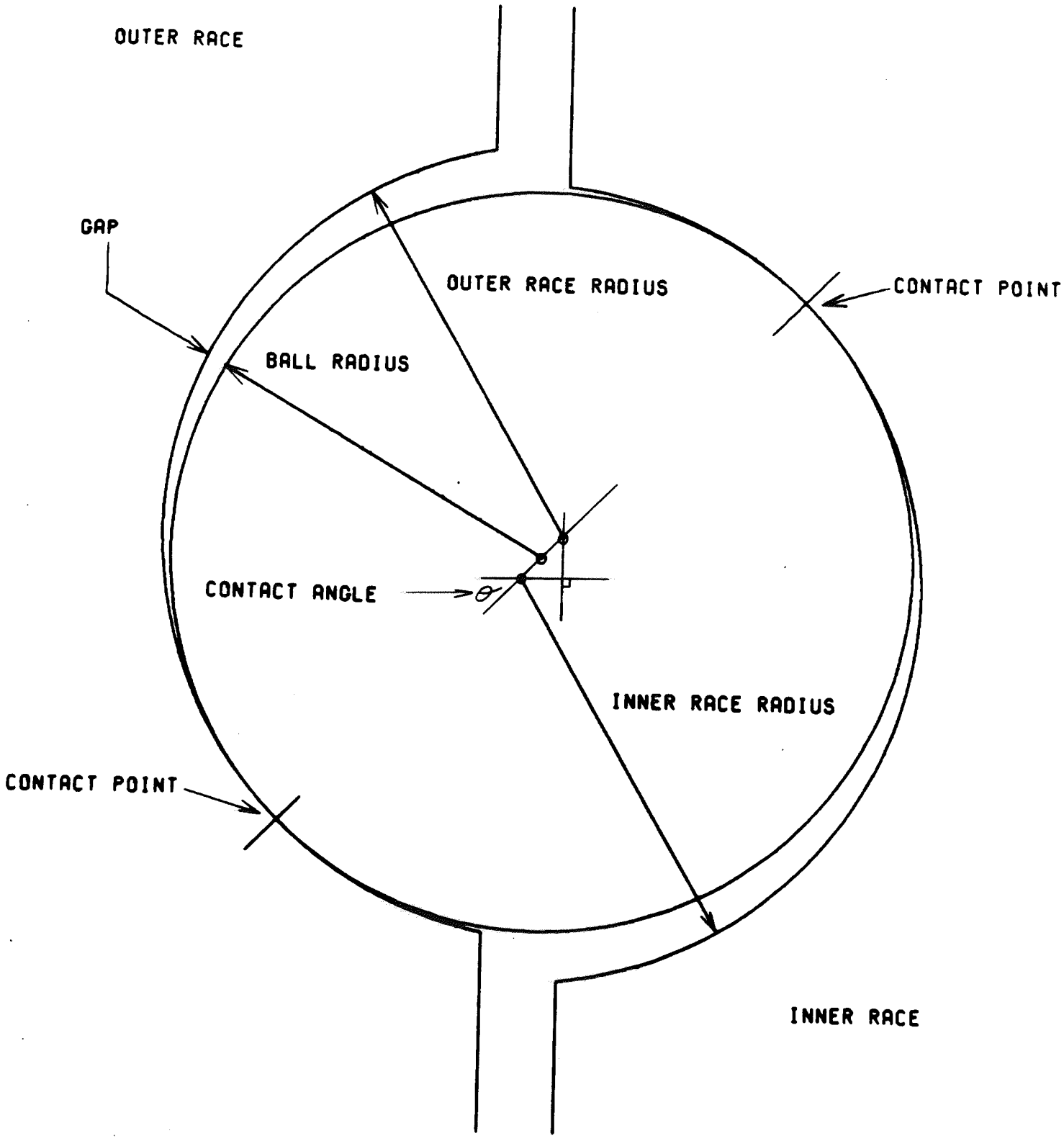

FIGURE 7

effected by race deformation. The above procedure was useful in that it gave good contact angle trends, but the contact angles were somewhat different from those in an actual bearing. This could be seen from the fact that at 90 degrees the contact angle dropped to zero over a range of the bearing circumference (Figure 8). This trend seemed highly unlikely with the presence of a load at 90 degrees. Considering the stiffness of the inner race relative to the outer race it was known that some of the load must pass from the inner race to the outer race at this location. A zero degree contact is not capable of carrying axial load. This was seen as a known inaccuracy but the contact angle plots were still of value.

The final stage of the analysis involved removal of the CBAR ball representation and actually modeling the balls with CGAP elements. This had two definite benefits. There would be no ball contact angle approximation which would in turn produce more accurate gap openings. In addition there would be no need for the radial elements because the balls would actually provide the radial stop. The CGAP elements were placed across the races as shown in figure 9. As can be seen in figure 9a, the inner and outer races have been constructed with nodes at discrete intervals along their race contours. Note that only the load bearing half of each race has been constructed in this manner. Six nodes were chosen to model these areas. The first node being at the 0 degree contact location and then a node at fifteen degree intervals to the edge of each race. Note that there is a node located at 45 degrees which represents the unloaded initial geometry of the bearing. This relatively coarse mesh was chosen for model simplicity but could be refined to obtain contact angles of greater accuracy. Once the gap elements were in place the appropriate gaps were calculated using bearing geometry with

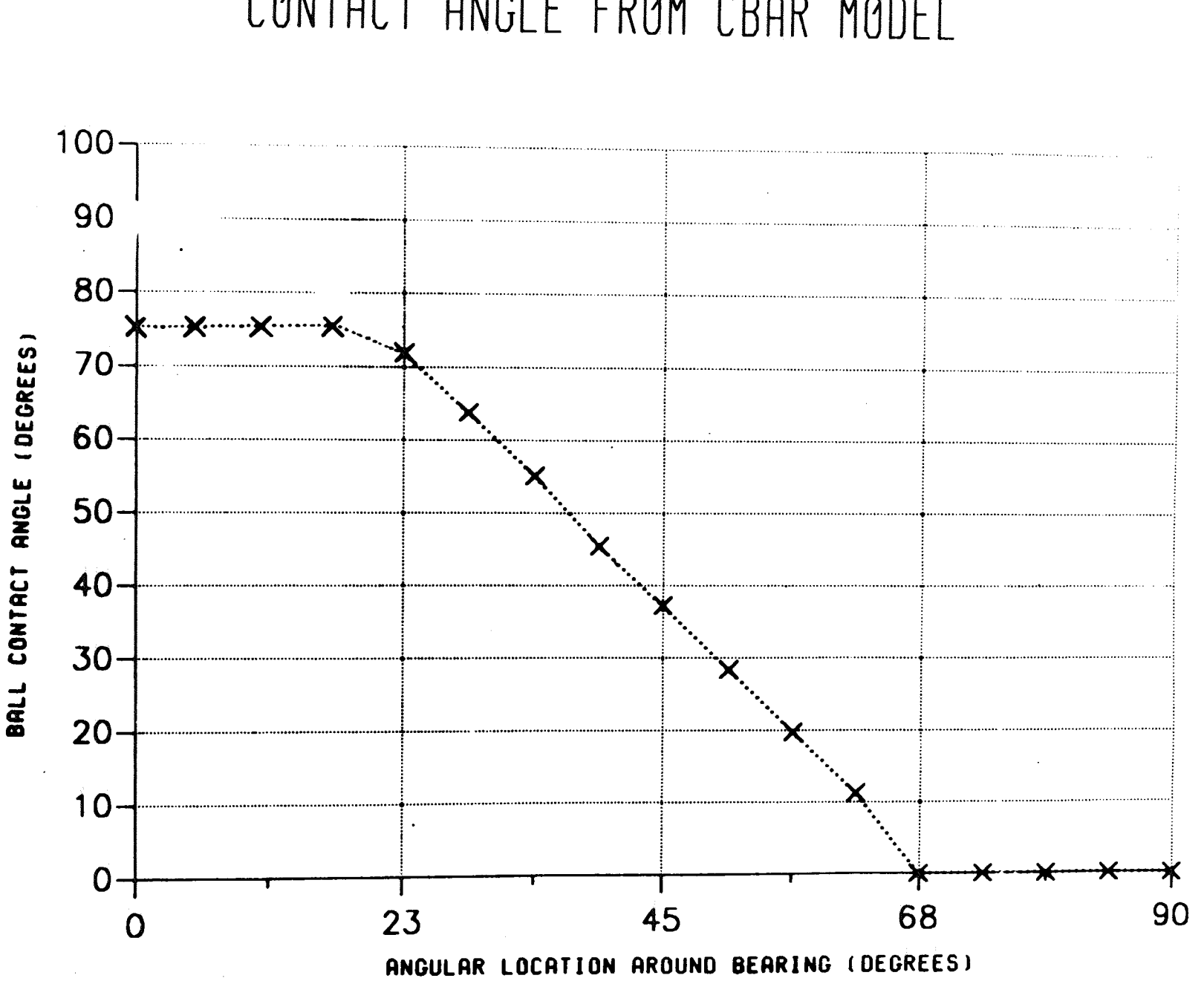
CONTACT ANGLE FROM CBAR MODEL
BALL CONTACT ANGLE (DEGREES)
100
90
80
70
60
50
40
30
20
10
0
0
23
45
68
90
ANGULAR LOCATION AROUND BEARING (DEGREES)

FIGURE 8

VARIABLE CONTACT BEARING CROSS SECTION

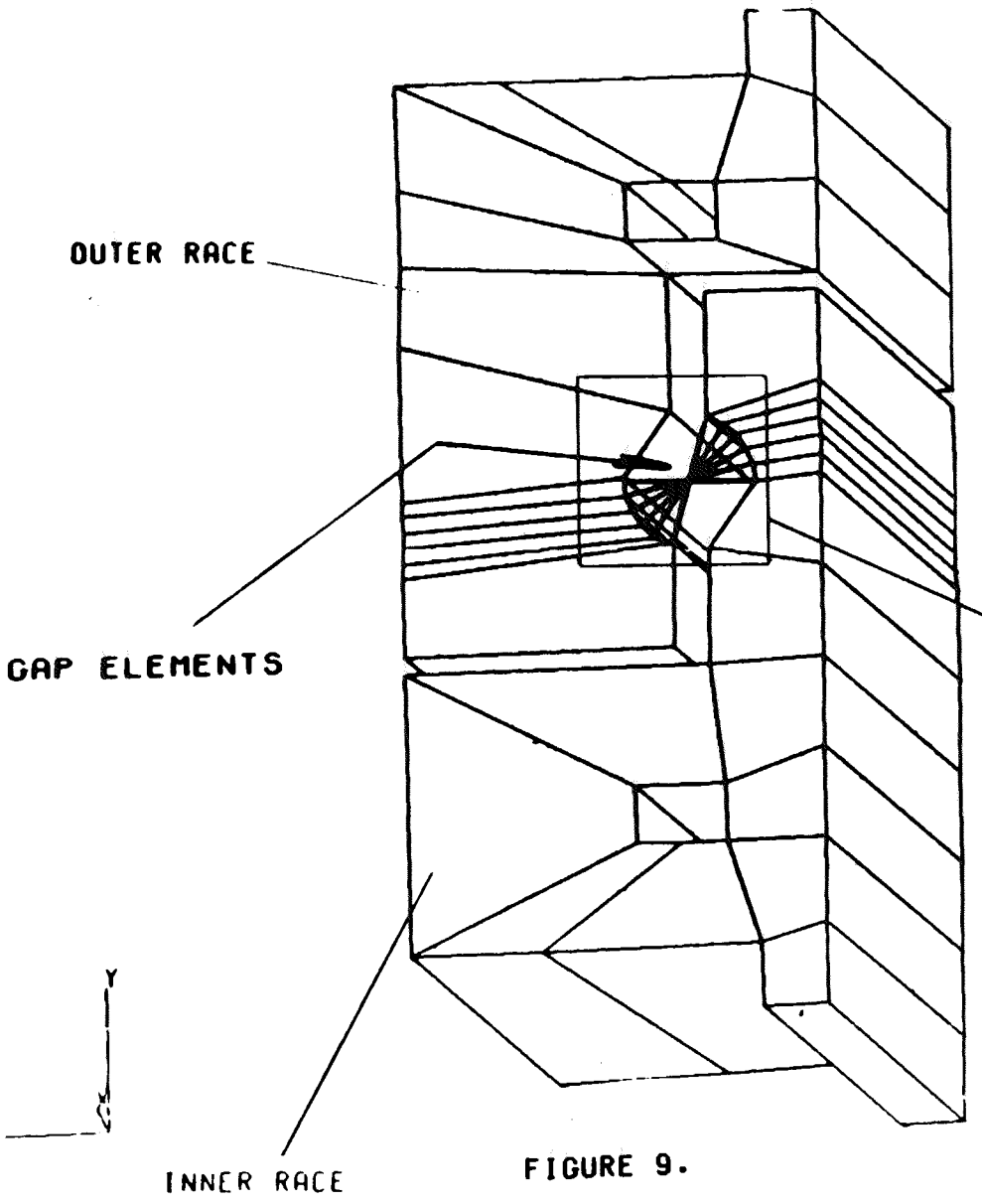

FIGURE 9.

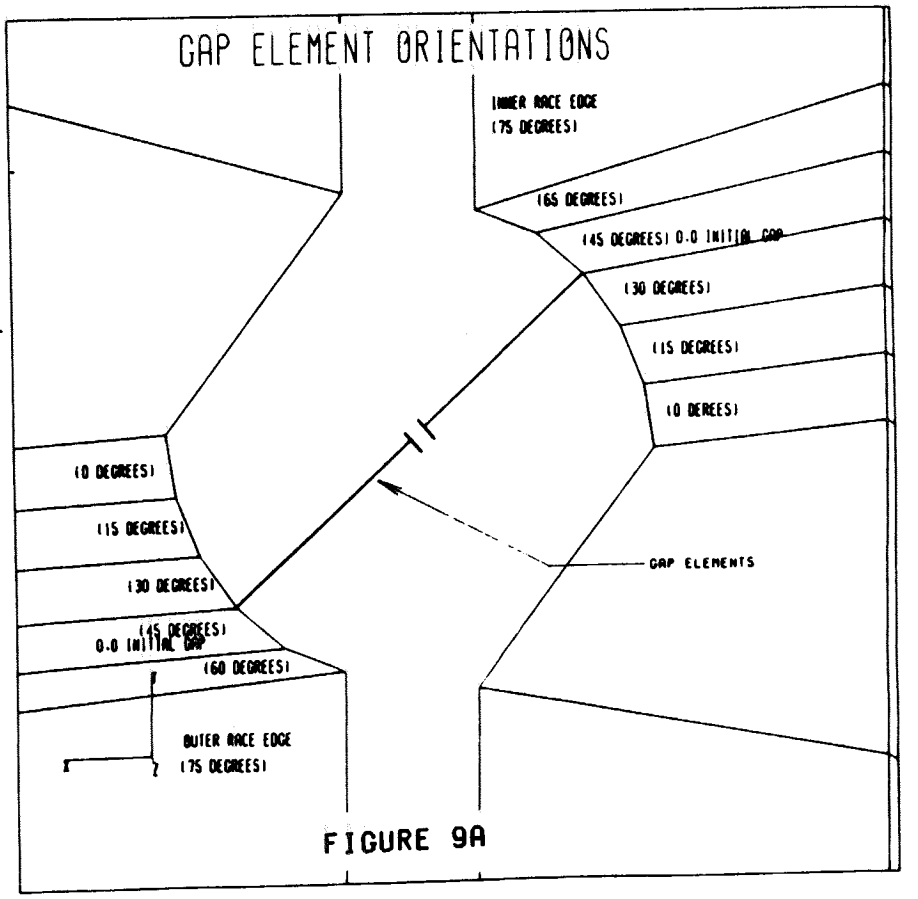

FIGURE 9A

the races and balls in initial contact with each other (figure 7).

The loading and boundary conditions were the same as in the other phases. In addition to paralleling previous load cases, various test cases were run. The loads and boundary conditions for the test cases were designed to yield contact angles that were predictable and thus verify the analysis technique.

The loads and boundary conditions of the two test cases can be seen in Figure 10. The first case involved uniform axial loading of the inner race and uniform axial constraint of the outer race. The second load case involved imposing uniform inward radial loading on the outer race and uniform outward radial loading on the inner race with the loading from test case 1. The results from this model configuration were promising and address some of the shortcomings of the previous phases.

IV. RESULTS:

For the first test case, contact angle for the various load increments was as expected. Upon initial application of the load, the contact angle was 45 degrees. As the load was increased the contact angle remained at 45 degrees until deformation of the races allowed the ball contact angle to shift to higher values. Note that although the contact angle shifted it remained constant around the races. This result was as expected.

The second set of verification loads were imposed on the first set. As the uniform radial loads were applied ball contact angle moved from 60 degrees down to 45 degrees. As the radial load was increased, the contact angle moved progressively down until the maximum load was reached and the contact angle stopped at a uniform 30 degrees. This

TEST CASE ONE

UNIFORM AXIAL RESTRAINTS

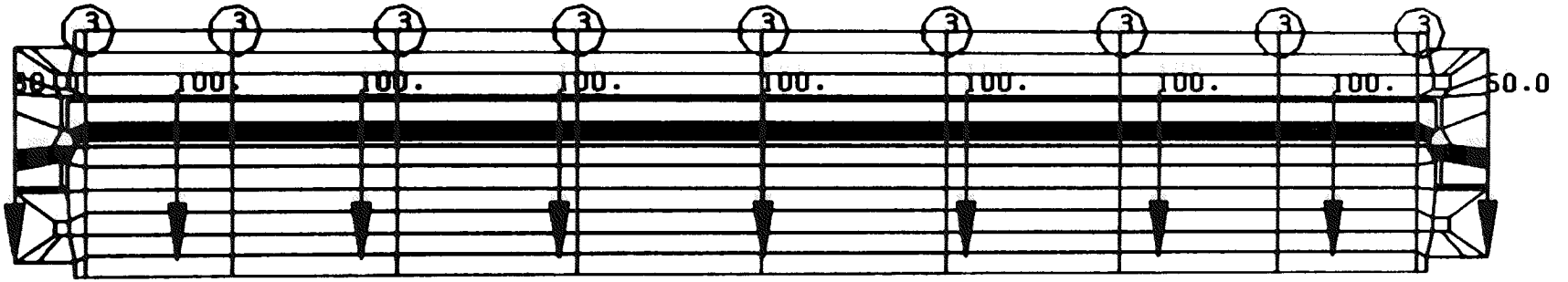

UNIFORM AXIAL LOADS

TEST CASE TWO

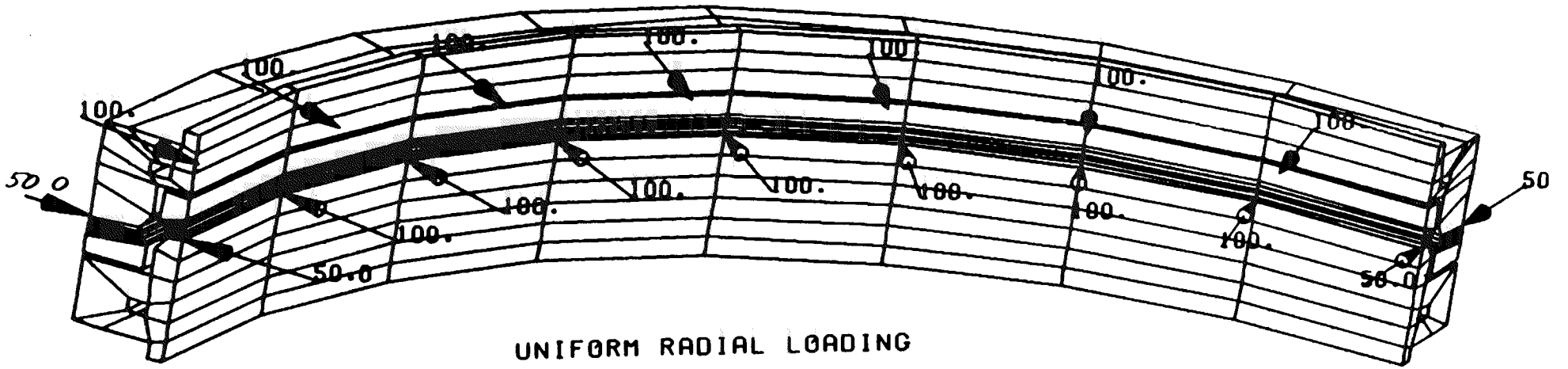

UNIFORM RADIAL LOADING

FIGURE 10

result was also expected.

The third load case was identical to those run in the earlier stages of the analysis. Four axial loads were applied to the inner race and two axial restraints were applied to the outer race. The results from this case looked very reasonable and explained some of the shortcomings in the earlier stages of the analysis.

Ball contact angle prediction had obvious improvements. The series of contact angle plots in Figure 11 show that all the balls contact at the same angle upon initial application of load and then ultimately become more positive at the 0 and 90 degree locations. This trend makes sense in that greater proportions of the load are transferred from the inner race to the outer race at these locations than at points between zero and 90 degrees. The contact angle plots in figure 11 show two phenomena not present in the earlier plots. The first being bands of contact in certain areas rather than a single line. This indicates that the true contact angle lies within these bands. The width of these bands could be reduced by increasing the number of CGAP elements representing the balls. The second phenomena present is "holes", or spaces, in the contact angle curves. These holes represent ranges of unloaded balls.

The contact angle plot of Figure 8 vs. the 745 pound load case of figure 11 shows the differences in ball contact angle between the CBAR model and the variable contact run. The greatest difference is between 45 and 90 degrees. The contact angle results from the CBAR run, as mentioned earlier, indicated that no load was transferred across the races at 90 degrees. Note that although the 45 degree CBAR elements carry axial load at 90 degrees the contact angle calculations do not reflect this. It can be seen from the variable contact model that the contact angle indicates a substantial load transfer at 90 degrees (Figure 12).

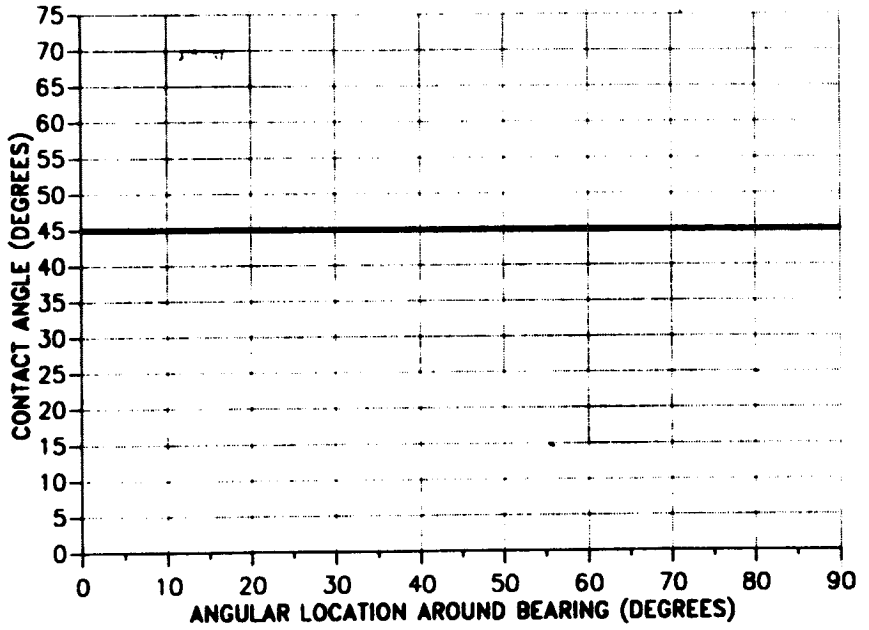
BALL BEARING CONTACT ANGLE
SUIT LOADING, 5 POUNDS
CONTACT ANGLE (DEGREES)
ANGULAR LOCATION AROUND BEARING (DEGREES)

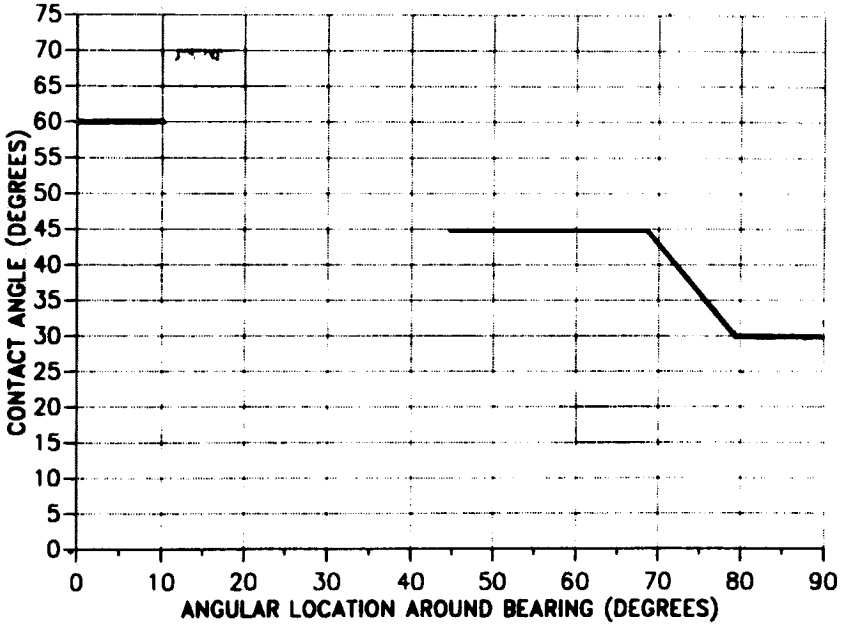
BALL BEARING CONTACT ANGLE
SUIT LOADING,200POUNDS
CONTACT ANGLE (DEGREES)
ANGULAR LOCATION AROUND BEARING (DEGREES)

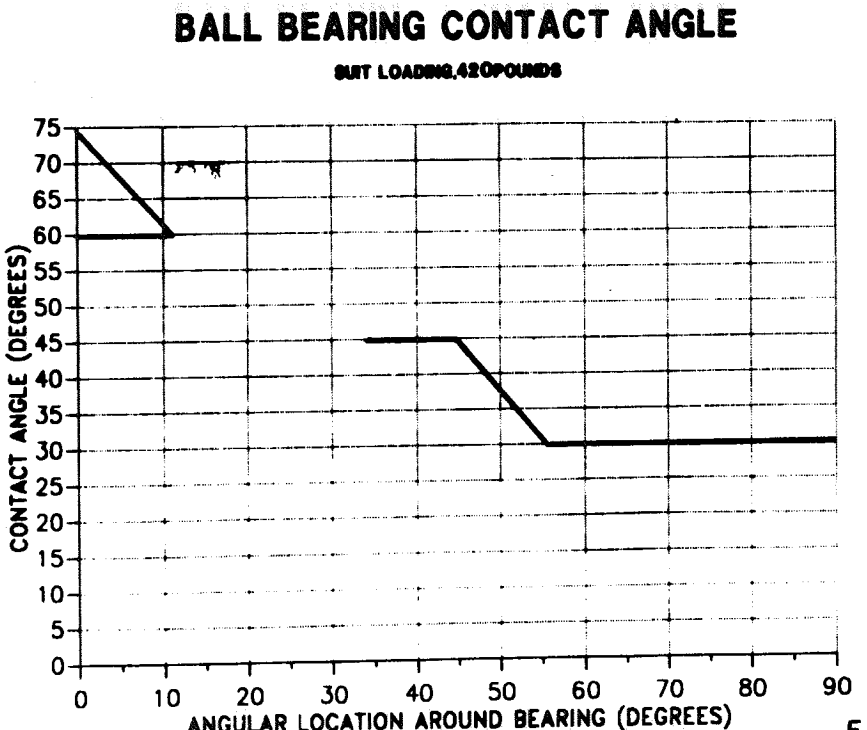
BALL BEARING CONTACT ANGLE
SUIT LOADING,420POUNDS
CONTACT ANGLE (DEGREES)
ANGULAR LOCATION AROUND BEARING (DEGREES)

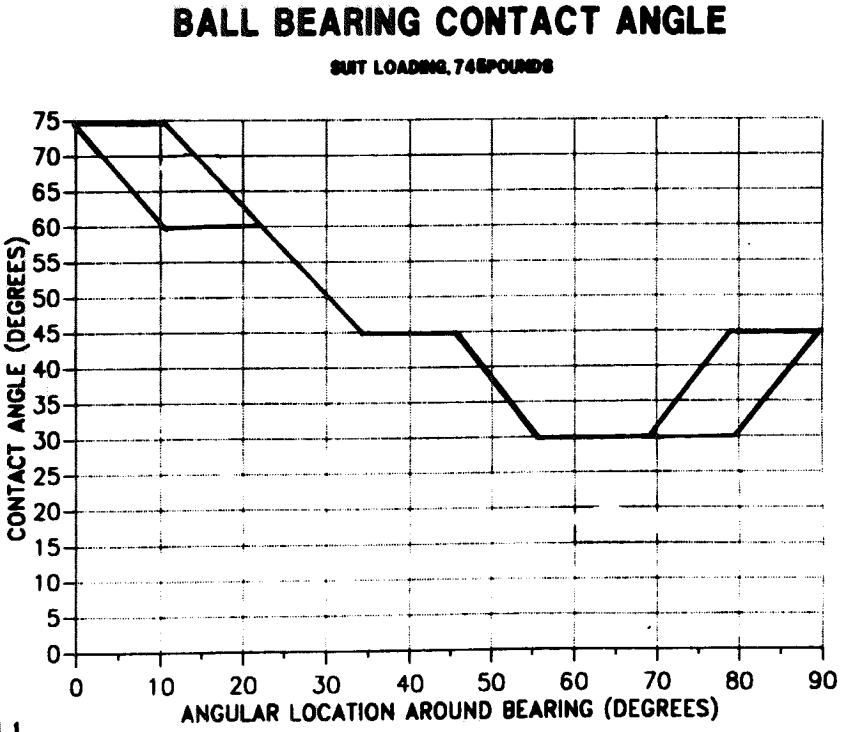
BALL BEARING CONTACT ANGLE
SUIT LOADING, 745POUNDS
CONTACT ANGLE (DEGREES)
ANGULAR LOCATION AROUND BEARING (DEGREES)

FIGURE 11

In addition it can be seen that large variations in contact angle occur around the races. This variation in contact angle serves to increase operating torque. This variation also leads to the earlier mentioned peaks in ball loading (Figure 12). Peaks in ball loading result in high contact stresses and again leads to increased bearing torque [1]. Variation of contact angle also results in variable radial gap opening around the bearing and as a result the pressure seals must be designed to accommodate the largest openings. This results in higher seal squeeze in areas away from the maximum opening.

Variation in contact angle is a result of the point loading of the bearing. The two point loading on the outer race and the four point loading on the inner race causes higher ball loading at the points of in line loads. As a result, an increase in radial gap occurs at these locations and a decrease occurs 90 degrees away. This decrease in gap represents an interference which drives the contact angle toward 0 degrees. This effect is offset somewhat by the inner races point load at this location but does not provide for uniform ball contact angle. As a result of the races taking oval shapes, the bearing undergoes a non-linear stiffening effect. This effect is apparent in figure 13. As the outer race deflects it tends to wrap around the inner race, thus causing the bearing system to become stiffer with increased deflection.

A test was conducted and bearing deflections were measured as the bearing system was loaded. Upon inspection of the races after testing it could be seen that the ball contact angle was following the same trends that the analysis was predicting. Deflections also closely followed trends predicted in the analysis. In addition, the deflection magnitudes bounded the test results for various load conditions.

FORCE DISTRIBUTION IN GAP ELEMENTS

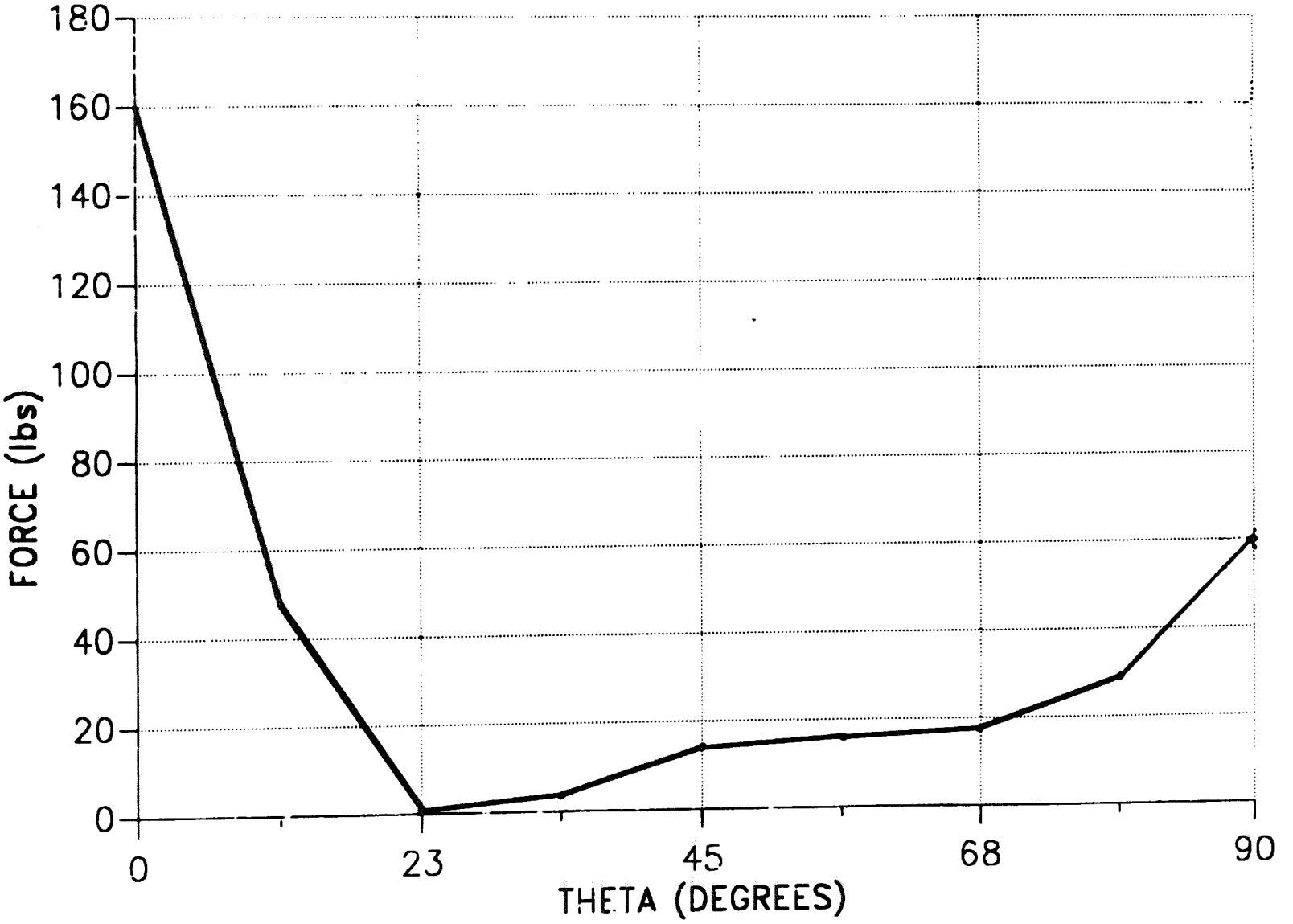

FIGURE 12

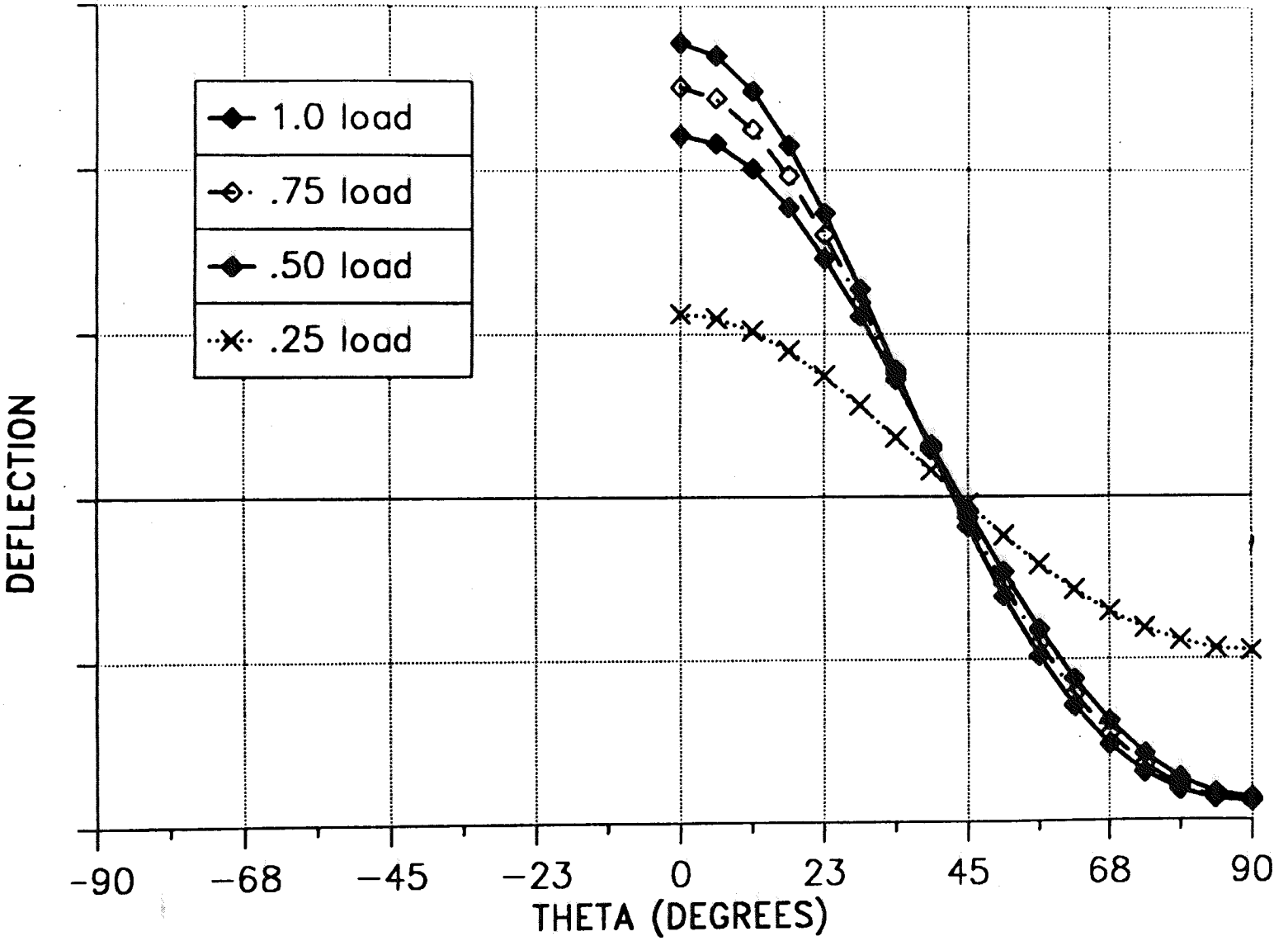
WAIST BEARING RELATIVE RADIAL DEFLECTIONS
1.0 load
.75 load
.50 load
.25 load
DEFLECTION
-90
-68
-45
-23
0
23
45
68
90
THETA (DEGREES)

FIGURE 13

V. CONCLUSION:

The use of the MSC/NASTRAN CGAP element and SOL66 has provided Hamilton Standard with a tool that has enabled designers to achieve a greater understanding of the behavior of these types of bearings.

It has become evident that under race deflection the races interfere due to their differential axial and radial deflections. When the outer race's radial deflection is restricted it stiffens due to circumferential tension. As a result the bearing is much stiffer than would be expected for individual races that do not interact through the ball/clearance action. As a consequence, changing the race material to one of a higher modulus does not result in a proportionately stiffer bearing.

From this analysis it is clear that there are significant variations in contact angle and ball loading which are a known causes of increased bearing torque and ball blocking [1]. In addition the insight into ball loading is useful in calculating ball/race contact areas. Ball contact area is of interest in evaluating torque and contact stress. This information has aided the designer in investigating new bearing configurations.

With the use of the above technique a redesign effort has been undertaken. This effort will include examination of numerous bearing configurations that will serve to optimize ball bearing torque through controlled ball loading, contact angle and seal squeeze. This redesign effort will be conducted primarily on the computer and once a final configuration is determined a test bearing will be constructed. This approach differs from previous approaches where test was the primary means of evaluating a new design. In addition to being of great aid in

the analysis of the waist bearing this technique has potential for additional applications.

This analysis technique may be used for other types of ball bearings , multilatch suit disconnects and the Ortman coupling, a joint commonly used in space related hardware. In addition, this method can be of use in the analysis of many structures that are coupled through deflection dependant geometry.

References:

[1]. Loewenthal, S.H, "Two Gimbal Bearing Case Studies: Some Lessons Learned", Lockheed Missiles and Space Co., Inc., Sunnyvale, California.